ORIGINAL ARTICLE

Elamipretide (SS-31) treatment attenuates age-associated post-translational modifications of heart proteins

Jeremy A. Whitson · Miguel Martín-Pérez · Tong Zhang · Matthew J. Gaffrey · Gennifer E. Merrihew · Eric Huang · Collin C. White · Terrance J. Kavanagh · Wei-Jun Qian · Matthew D. Campbell · Michael J. MacCoss · David J. Marcinek · Judit Villén · Peter S. Rabinovitch [ORCID]

Abstract It has been demonstrated that elamipretide (SS-31) rescues age-related functional deficits in the heart but the full set of mechanisms behind this have yet to be determined. We investigated the hypothesis that elamipretide influences post-translational modifications to heart proteins. The S-glutathionylation and phosphorylation proteomes of mouse hearts were analyzed using shotgun proteomics to assess the effects of aging on these post-translational modifications and the ability of the mitochondria-targeted drug elamipretide to reverse age-related changes. Aging led to an increase in oxidation of protein thiols demonstrated by increased S-glutathionylation of cysteine residues on proteins from Old (24 months old at the start of the study) mouse hearts compared to Young (5–6 months old). This shift in the oxidation state of the proteome was almost completely reversed by 8 weeks of treatment with elamipretide. Many of the significant changes that occurred were in proteins involved in mitochondrial or cardiac function. We also found changes in the mouse heart phosphoproteome that were associated with age, some of which were partially restored with elamipretide treatment. Parallel reaction monitoring of a subset of phosphorylation sites revealed that the unmodified peptide reporting for Myot S231 increased with age, but not its phosphorylated form and that both phosphorylated and unphosphorylated forms of the peptide covering cMyBP-C S307 increased, but that elamipretide treatment did not affect these changes. These results suggest that changes to thiol redox state and phosphorylation status

J. Whitson · P. Rabinovitch (✉)
Department of Pathology, University of Washington, 1959 NE Pacific St, Seattle, WA 98195, USA
e-mail: petersr@u.washington.edu

Present Address:
J. Whitson
Department of Biology, Davidson College, 405 N Main St, Davidson, NC 28035, USA

M. Martín-Pérez · G. Merrihew · E. Huang · M. MacCoss · J. Villén
Department of Genome Sciences, University of Washington, 3720 15th Street NE, Seattle, WA 98195, USA

T. Zhang · M. Gaffrey · W.-J. Qian
Integrative Omics, Pacific Northwest National Laboratory, 902 Battelle Boulevard, Richland, WA 99352, USA

C. White · T. Kavanagh
Department of Environmental & Occupational Health Sciences, University of Washington, 4225 Roosevelt Way NE, Seattle, WA 98105, USA

M. Campbell · D. Marcinek
Department of Radiology, University of Washington, 1959 NE Pacific St, Seattle, WA 98195, USA

are two ways in which age may affect mouse heart function, which can be restored by treatment with elamipretide.

Introduction

Alteration of protein post-translational modifications (PTMs) is a well-established mechanism of cellular aging [1–3]. These alterations contribute to age-related dysfunction in many tissue and organ systems, including the heart which has been shown to have altered PTM profiles with age [4]. These age-associated changes could contribute to cardiac pathologies, the leading cause of death in elderly populations [5, 6].

Age-related changes to PTMs include both enhancement and loss of modifications to various residues. Greater oxidative stress in the cell, primarily due to elevated mitochondrial oxidant production, is a major source of PTMs that are elevated with age [2, 7]. Among the most common oxidative modifications is reversible S-glutathionylation, including those due to the actions of glutathione-utilizing defense mechanisms that are required to prevent harmful forms of reactive oxygen species (ROS) from damaging proteins [8]. S-glutathionylation can thus be viewed as a marker of general protein oxidation. We have demonstrated that mouse hearts show increased oxidative stress [5] and enhancement of S-glutathionylated residues with age [4].

Aging also leads to dysregulation in the phosphorylation of various residues that play an important role in signaling and cellular regulation [2]. We have previously shown that changes in the phosphorylation of key residues in cardiac myosin binding protein C (cMyBP-C) and cardiac troponin I (cTnI) appear to be major contributors to the age-related loss of diastolic function in the mouse heart [4].

Restoration of proper PTM profiles has been proposed as one way to repair function in old age. Since much of this dysregulation originates from altered mitochondrial energetics and ROS, drugs that improve mitochondrial health have a strong potential to restore

PTM balance. Elamipretide (also referred to in the past as SS-31) is a mitochondrial-targeted drug that we have previously shown to be effective at restoring function in old mouse hearts [9]. One mechanism by which elamipretide achieves this effect is by modifying PTM profiles, including enhanced cMyBP-C phosphorylation and decreased global S-glutathionylation [4]. These changes are likely secondary to its primary effect of associating with the cardiolipin-rich mitochondrial inner membrane where it improves the efficiency of the electron transport chain and other mitochondrial proteins and reduces the leak of reactive species [9–13].

To investigate the hypothesis that elamipretide's effects on cardiac function are influenced by changes in S-glutathionylation and phosphorylation of heart protein residues, both at the level of individual proteins and across biological pathways, we used a shotgun proteomics approach to compare phosphoproteomes and thiol proteomes of Young, Old, and Old mouse hearts treated with elamipretide (Old+ELAM). We present here the first large-scale analysis of S-glutathionylation and phosphorylation of aged mouse heart proteins, providing detailed information on thousands of proteins across hundreds of biological pathways.

Results

Elamipretide treatment restores the thiol redox proteome to more youthful state

Quantitative analysis of protein S-glutathionylation was performed by mass spectrometry, as previously described [10]. Aging resulted in a broad increase in S-glutathionlyation that was reversed by elamipretide (referred to as ELAM in figures and tables) treatment (Fig. 1A, B). The 50 age-related S-glutathionylation changes with the lowest P-values are shown in Table 1 and the full set of results can be viewed in Appendix 1. A histogram of the S-glutathionylation occupancy measured at the peptide level illustrates an age-related increase in S-glutathionylation and shows that the elamipretide treatment in Old mice produced a general shift in S-glutathionylation almost completely back to the Young state (Fig. 1C). Canonical pathway analysis by Ingeniuty Pathway Analysis (IPA) software (QIAgen) also shows that many of the significantly

affected pathways are linked to mitochondria and/or aging, such as sirtuin signaling, oxidative phosphorylation, mitochondrial dysfunction, TCA cycle, and NRF2-mediated oxidative stress response and that elamipretide treatment was effective at restoring the youthful state of the thiol proteome across the effected pathways, as evident by the similarities of the heatmaps (Fig. 1D). Heatmap visualization of S-glutathionylation differences in peptides of selected pathways further demonstrates that elamipretide treatment strongly and uniformly shifted the oxidation state of the heart proteome back to that of Young mice (Fig. 1E). Our results also show extensive S-glutathionylation of proteins involved in cardiomyocyte elasticity, such as titin, and that elamipretide greatly reduces the S-glutathionylation of these residues in aged hearts (Appendix 1, Table 1).

The global trend seen in S-glutathionylation by proteomics was further confirmed by an HPLC assay (Fig. 1F). This analysis demonstrates that bulk S-glutathionylation, measured as glutathione (GSH)/protein after isolation and reduction, was decreased significantly ($P < 0.05$) in the heart following elamipretide treatment.

### Phosphoproteomics reveals age-related changes and elamipretide effects

We previously described age-based changes to a small set of phosphorylation sites that are important for cardiac function [4]. To determine additional phosphosites that may regulate heart function, we analyzed the global phosphoproteome of Young, Old, and Old elamipretide-treated mouse hearts. The 50 differences between groups with the lowest P-values are shown in Table 2 and the full phosphoproteomic results can be found in Appendix 2. Many sites were identified with changes between groups of unadjusted P-value < 0.05 (Fig. 2A, B).

Canonical pathway analysis by IPA shows that elamipretide had a significant effect on many of the pathways that were altered with age and play a known role in cardiac function, such as ILK signaling, protein kinase A signaling, rhoA signaling, and actin cytoskeleton signaling (Fig. 2C). However, when assessing the individual phosphosites involved these pathways, we found that the Young and Old Control hearts tended to cluster more closely together than with the Old + elamipretide hearts (Fig. 2D).

To fully contextualize the phosphoproteome results, we also quantified the unmodified proteomes of the same set of samples (Fig. 3A, B). The 50 differentially regulated proteins with the lowest P-values are shown in Table 3 while the full proteome results can be found in Appendix 3. Canonical pathway analysis by IPA revealed that affected pathways were largely related to cell signaling, metabolism, and structure, with limited overlap between the pathways identified in the phosphorylation data (Fig. 3C). In most pathways, the Old Control and Old + elamipretide results clustered more closely together than with the Young, though the mitochondrial dysfunction pathway was a notable exception to this (Fig. 3D).

The limited overlap between the significantly altered pathways in the phosphoproteomic and proteomic datasets, and the differential clustering of the groups, indicates that most of the changes found in the phosphoproteome are driven by changes in signaling and phosphoregulation of these proteins rather than differences in protein abundance.

Based on the large-scale phosphoproteomic results, we selected a subset of phosphorylation sites for further targeted analysis by parallel reaction monitoring to better assess whether they play a role in the regulation of the aging heart and restoration of function by elamipretide. These targets were selected from sites that showed an unadjusted P-value < 0.05 in the large-scale phosphoproteomic analysis presented here, as well as sites of interest identified in our prior study [4]. These targets included phosphorylation sites on titin (Ttn), actinin alpha 2 (Acta2), cMyBP-C, myotilin (Myot), cardiac phospholamban (Pln), heat shock protein family B member 6 (HSPB6), and creatine kinase M-type (Ckm). As shown in Fig. 4, we found different abundance for many phosphosites in the Young and Old groups, and some differences were significant. However, elamipretide did not appear to have any significant effects on the phosphorylation of these sites. Notably, we observed an increase in the unmodified cMyBP-C containing Ser307 with age ($P = 0.074$) while the corresponding phosphopeptide did not change (Fig. 4F). This suggests that the phosphorylation site has high stoichiometry given that there was no change in abundance when all cMyBP-C peptides were aggregated (Appendix 3). Conversely, Myot showed significant age-related increases in both phosphorylated and unmodified peptides containing the Ser231 site (Fig. 4G, H), indicating the change observed in phosphorylation is
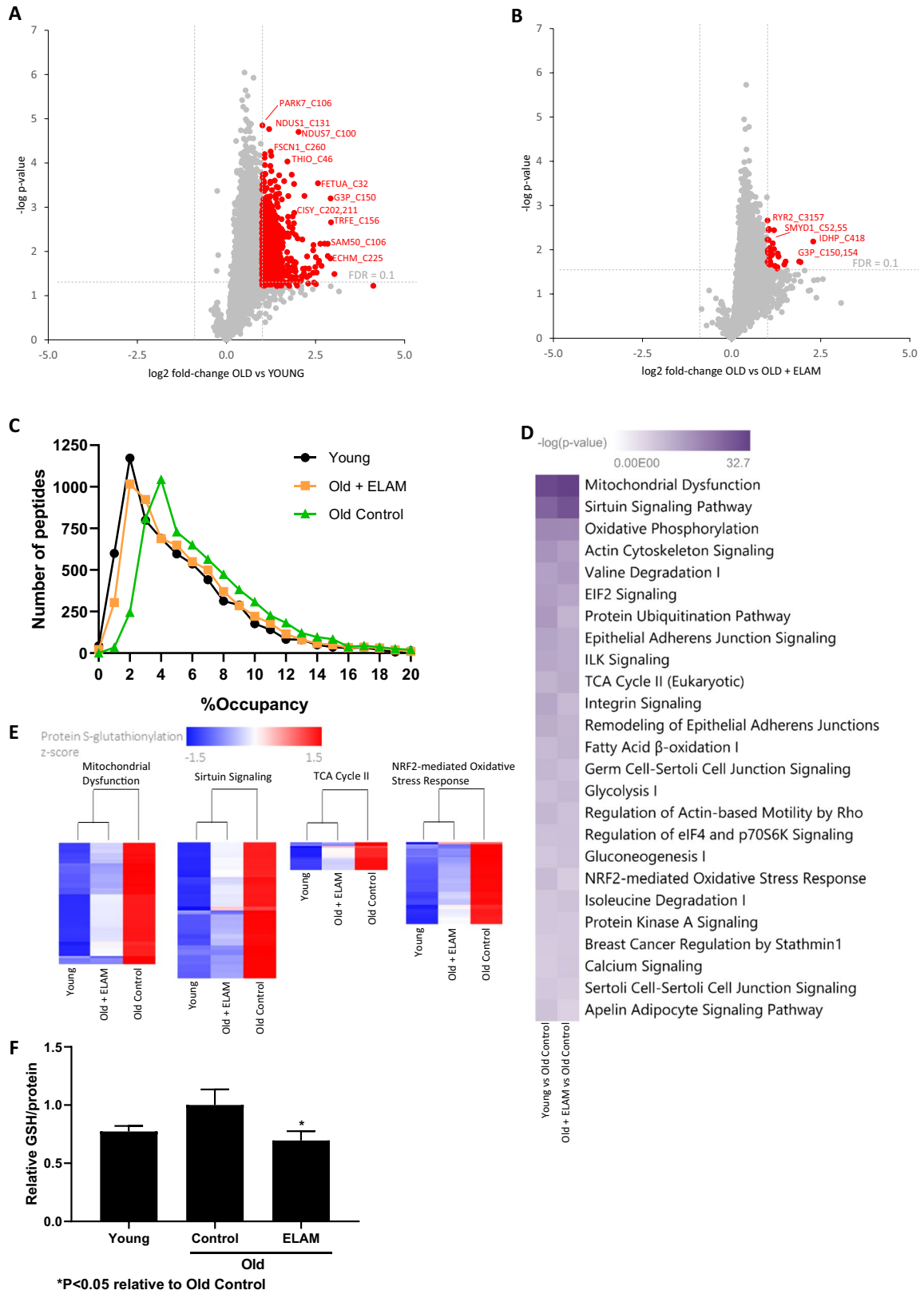
◀**Fig. 1** Analysis of protein S-glutathionylation in mouse hearts. (**A**, **B**) Volcano plots of protein S-glutathionylation analysis. Each dot represents one detected peptide. The horizontal dotted line indicates FDR = 0.01. The vertical dotted lines represent log2 ratios > 1 and < − 1. (**C**) Histogram of %occupancy of cysteine residues on detected peptides. (**D**) *P*-value heatmap of protein S-glutathionylation changes in canonical pathways based on all changes with an unadjusted *P* < 0.05. Top 25 pathways, ranked by *P*-value, are shown. (**E**) Row-normalized z-score heatmaps of significant (*P* < 0.05) S-glutathionylation differences in selected pathways. (**F**) Mean GSH bound to protein by treatment group normalized to Control, as determined by HPLC. *N* = 5 for all groups

due to changes in protein expression. The full set of PRM results, including peptide sequences used, is provided in Table 4 while additional information on the sample list and peptide inclusion can be found in Appendix 4.

Supplemental data

Full proteomic datasets can be found in the following appendices:

    Appendix 1: S-Glutathionylation Proteomics Results
    Appendix 2: DDA Phosphoproteomics Results
    Appendix 3: DDA Proteomics Results
    Appendix 4: PRM Phosphoproteomics Sample List and Peptide Inclusion

Raw data and Skyline document (ProteomeXchange ID: PXD024247) for PRM phosphorylation measurements is available at Panorama (https://panoramaweb.org/SS31PTM.url). Raw data for S-glutathionylation is available at MassIVE (ftp://massive.ucsd.edu/MSV000085329/). Raw data for large-scale DDA proteomics and phosphoproteomics have been deposited in the ProteomeXchange Consortium via the PRIDE partner repository with the dataset identifier PXD026335 [14].

Additional figures showing the results of statistical analyses are available in the Supplemental Data document.

Discussion

Mitochondrial thiols are heavily oxidized with age but elamipretide rapidly reverses these changes

Our data reveal a near universal shift in heart protein thiol oxidation state with age. This is consistent with the redox stress hypothesis, which states that the loss of function that occurs with age is due to a shift in the redox state of cells to more oxidizing conditions, resulting in protein thiols becoming oxidized and disrupting signaling and other important functions of these proteins [15]. Elamipretide treatment appeared to rapidly restore the environment of cardiomyocytes to a less oxidizing state and reversed the majority of the age-related S-glutathionylation after 8 weeks of treatment. Of the 4180 significantly (FDR < 0.1) altered sites when comparing Young to Old Control, which exclusively showed enhanced S-glutathionylation with age, only 7 also demonstrated a significant difference between Young and Old + elamipretide (Appendix 1). This illustrates how uniform the effect of age is on S-glutathionylation, and how effective elamipredite is at reversing this change.

The S-glutathionylation data also appear to show an overrepresentation of mitochondrial proteins based on our pathway analysis. Given that mitochondria are the largest contributor of reactive oxygen species in the cell, it is not surprising that these pathways were heavily affected and implies potential damage to mitochondrial proteins. Although the effects of S-glutathionylation are site-specific and unknown in most cases, alteration of mitochondrial protein thiol oxidation state may explain our previous finding that elamipretide and nicotinamide mononucleotide (NMN), a NAD⁺ precursor, had a greater effect on mitochondrial metabolism in the aged heart when the two were administered simultaneously than either alone [9]. In that study, we determined that NMN or elamipretide administered alone did not normalize age-related alterations to mitochondrial NAD(H) flux in response to increased workload but that the combination of the drugs did have a restorative effect. This could be due to changes in signaling and/or enzyme activity along mitochondrial pathways resulting from the difference in S-glutathionylation state, especially TCA cycle enzymes which control NAD(H) flux and show large differences in S-glutathionylation.

In addition to the reported correlation between phosphorylation changes and diastolic heart function [4], there are indications that oxidative changes may also contribute to elamipretide's improvement of diastolic function in aged hearts. A recent study has revealed that cardiac stiffness is heavily influenced by the oxidation of cysteine residues along titin [16], and many of these same residues showed enhanced

Table 1 Top 50 age-related S-glutathionylation changes in mouse hearts. Bold numbers indicate significance (FDR < 0.1). Ordered by lowest *P*-value in Young vs Old Control comparison. Full results can be found in Appendix 1

Peptide	Maps to protein	Fold change relative to old control	
		Young	Old ELAM
K.VCIVGSGNWGSAIAK.I	Gpd1	**−1.42**	**−1.20**
R.SNTGGQAFPQCVFDHWQILPGDPFDNSSRPSQVVAETR.K	Eef2	**−1.69**	**−1.18**
R.YADLTEDQLPSCESLKDTIAR.A	Pgam1	**−1.45**	**−1.22**
R.GFLTERDDILCPDCGKDI.-	Fhl2	**−1.51**	**−1.35**
K.AEFASACTPGLHVDLSAAGSEIKPEVSSSMPAAVDVLR.T	Perm1	**−1.36**	−1.23
R.WGLGGTCVNVGCIPK.K	Txnrd1	**−1.39**	**−1.19**
K.CEFDPLHTVLLK.D	Cobll1	**−1.47**	**−1.33**
R.LDGNPLTQSSLPPDMYECLR.V	Lum	**−1.46**	**−1.25**
R.HLLPLVQCPTLIVHGEKDPLVPR.F	Bphl	**−1.49**	**−1.41**
R.AGKPVICATQM*LESMIK.K	Pkm	**−1.53**	**−1.28**
K.SSFATPGVNVGLFCSTPAVALGR.A	Echdc3	**−1.56**	**−1.28**
K.CNENYTTDFIFNLYSEEGK.G	Pfkm	**−1.61**	**−1.39**
K.GLIAAICAGPTALLAH.E	Park7	**−2.01**	−1.77
R.KTETVCTFQDGALVQHQQWDGK.E	Fabp5	**−1.57**	**−1.34**
R.EGVM*EFLLANHPLDC#PICDQGGEC#DLQDQSMMFGSDR.S	Ndufs1	**−2.30**	−1.53
K.VIDVTVPLQCLVK.D	Dnajc11	**−1.49**	**−1.32**
R.PFDIRTECFVPDDKEEYVK.A	Myh6	**−1.32**	−1.27
K.EKPYFPIPEDCTFIQNVPLEDR.V	Hnrnpu	**−1.52**	**−1.29**
K.SSAAQAIHPGYGFLSENMEFAELCK.Q	Mccc1	**−1.46**	**−1.27**
K.LCYVALDFENEM*ATAASSSSLEK.S	Acta2	**−1.58**	**−1.37**
R.SSLWPMTFGLAC#CAVEMMHMAAPR.Y	Ndufs7	**−4.07**	−2.30
K.YGALVICETPEQIANLEEVGR.R	Tsfm	**−1.57**	**−1.29**
K.KWDTCAPEVILHAVGGK.L	Bpnt1	**−1.69**	**−1.48**
R.QELQVIADLCVK.H	Kyat3	**−1.40**	**−1.25**
K.SLCPETWPMWAGRPQDGVAVLVR.H	Myo1c	**−1.46**	−1.35
R.SAVQYAECQSK.A	Manba	**−1.21**	−1.17
R.IDVAVNCAGIAVAIK.T	Hsd17b10	**−1.95**	**−1.52**
K.ELLFYCSLPQSR.E	Snta1	**−1.45**	**−1.36**
K.DIRVCLVEK.A	Etfdh	**−1.65**	**−1.42**
R.SCQTALAEILDVLVR.A	Iars2	**−1.61**	−1.45
K.LCYVALDFEQEM*ATAASSSSLEK.S	Actb	**−1.69**	**−1.41**
K.TVVNISSLCALQPYK.G	Spr	**−1.54**	**−1.32**
K.STQFEYAWCLVR.S	Fis1	**−1.44**	**−1.28**
K.CAELEEELK.T	Tpm1	**−1.66**	−1.22
K.VGKDELFALEQSCAQVVLQAANER.N	Fscn1	**−2.37**	**−1.76**
K.MLTEAIMHDCVVK.L	Eif4g1	**−1.50**	**−1.32**
K.KLNCQVIGASVDSHFCHLAWINTPK.K	Prdx1	**−1.40**	**−1.26**
K.ALAGCDFLTISPK.L	Taldo1	**−1.76**	−1.38
K.LTHAAPCMLFMK.G	Glrx3	**−1.33**	**−1.21**
K.SGSTVFAEIQGVIDACIK.L	Ap3m1	**−2.10**	**−1.77**
K.NDPPMEAAGFTAQVIILNHPGQISAGYAPVLDCHTAHIACK.F	Eef1a1	**−1.48**	**−1.29**
R.CNSVLPGFIATPMTQK.M	Hsd17b8	**−1.37**	**−1.21**
K.CPKPVIAAIHGGCIGGGVDLVSACDIR.Y	Ech1	**−1.42**	**−1.27**

Table 1 (continued)

Peptide	Maps to protein	Fold change relative to old control	
		Young	Old ELAM
R.NAGIEAQVWKPSFCFK.-	*Synpo*	−1.91	−1.54
K.ISNVGEDSCTVQWEPPAYDGGQPVLGYILER.K	*cMyBP-C*	−1.46	−1.31
K.TGQATVASGIPAGWMGLDCGTESSKK.Y	*Pgk1*	−1.37	−1.18
K.TYILTCEHDVLRDDGIMYAK.R	*Nceh1*	−2.40	−1.67
R.ILEGMGVTFHCK.M	*Ttn*	−1.48	−1.32
K.ILDVGCGGGLLTEPLGR.L	*Coq3*	−1.55	−1.28
R.KGLIAAICAGPTALLAHEVGFGCK.V	*Park7*	−2.10	−1.69

S-glutathionylation with age that was reversed by elamipretide treatment in our analysis. The combined lower oxidation of essential mitochondrial and cardiac proteins may be one of the core mechanisms by which elamipretide is able to drastically improve the function of aged hearts.

Notably, these results are similar to what we had previously reported in skeletal muscle tissue, where we showed the same global shift in thiol redox status, with essential muscle and mitochondrial proteins being most affected with age and rapidly repaired by elamipretide [10]. Thus, our findings in heart may have broader implications for other muscle and mitochondrion-rich tissues, warranting additional study.

While elamipretide has been clearly demonstrated to restore the redox state of aged muscle tissues to a near-young state, it has yet to be determined whether this can affect more persistent oxidative modifications of proteins beyond reversible S-glutathionylation, which may also greatly impact tissue function.

How does elamipretide regulate phosphorylation?

Phosphoproteome data were not expected to show the same global shift that the S-glutathionylation data did, given the more selective mechanisms of regulation of protein phosphorylation. We report many new sites of interest that should be further examined to gain insight into how heart protein phosphorylation changes with age and the degree of elamipretide's effect on reversing these changes. Furthermore, combining these phosphorylation results with protein abundance results demonstrates that the phosphorylation changes cannot generally be owed to a difference in protein abundance that maintains the same proportion of phosphorylation

and instead represent true regulatory changes in phosphorylation status. Intriguingly, while elamipretide significantly affected phosphoregulation in many of the same pathways that aging did, the actual phosphosites impacted were often different, to the point where the phosphorylation profile of elamipretide-treated Old hearts often looked more different from Young hearts than untreated Old hearts did (Fig. 2D). This seems to indicate that, while elamipretide has a restorative effect on the level of pathways and function impacted by aging, it is not always restorative at the level of individual phosphosites impacted by aging. Rather, there are many cases where elamipretide enhanced phosphorylation of residues that were not affected by age at all, while, conversely, it did not significantly alter the most robust age-related changes in phosphorylation (Table 2).

The question also remains of how exactly elamipretide regulates phosphorylation given that there is no direct mechanism by which it can phosphorylate or dephosphorylate proteins. The most obvious explanation for the elamipretide treatment's effect on phosphoregulation is that it results in modulation of kinase and phosphatase activity or abundance. Sites along many phosphatases and phosphatase regulators, such as PP1B, PP14C, PP2AA, and PP2BA and kinases, such as MAPK1, MAPK12, MAPK14, and PDK1, had significantly altered S-glutathionylation with age and elamipretide treatment (Appendix 1). On the level of abundance, PDK2 was the only phosphoregulator significantly affected by age, but with only a modest 1.45-fold downregulation and no significant effect by elamipretide (Appendix 3). Thus, the data we have presented here suggests that elamipretide's impact on phosphorylation could be influenced by its alteration

Table 2 Top 50 age-related phosphorylation changes in mouse hearts. Bold indicates unadjusted P-value < 0.05. Ordered by lowest P-value in Young vs Old Control comparison. Full results can be found in Appendix 2

Peptide (@ indicates site of phosphorylation)	Maps to protein phosphorylation site(s)	Fold change relative to old control	
		Young	**Old ELAM**
DALLGSNPNKPS@PPSSPSSR	*Myom1_S863*	**3.53**	−1.12
ILNPAAIPEGQFIDS@R	*Myh6_S740*	**1.29**	1.41
SNLKPDVEHCTGAGTGS@PLEEEVR	*Rbpms2_S18*	**−1.77**	−1.06
GAPVPSTGAPPS@PK	*Naca_S765*	**−2.00**	1.04
GIS@LEEGALPDVSATR	*Xirp1_S295*	**2.09**	1.06
GAPNALAESPAS@PK	*Naca_S1285*	**−1.96**	1.01
KAS@LKDSGEYTCETEASK	*Obscn_S3321*	**1.94**	1.24
TVS@QESLTPGKLEINFEQLLR	*Nexn_S296*	**−2.07**	−1.53
IYSHS@GEDIEFGCK	*Cfh_S1198*	**2.85**	1.40
VMHTQCHSTPDS@AEDVRK	*Ahsg_S138*	**1.86**	1.02
SGS@PGPLHSVSGYK	*Rbm20_S728*	**−1.37**	−1.26
VDNARVS@PEVGSADVASIAQK	*Fam21_S747*	**1.34**	−1.07
LLTRT@PDIAQR	*Stk39_T366*	**−2.21**	−1.36
GDS@ETDLEALFNAVMNPK	*Yap1_S46*	**1.79**	−1.06
TYS@LGSALRPSTSR	*Vim_S39*	**3.40**	1.35
GRS@SLDLDKTPAFLHVK	*Nebl_S352*	**1.89**	1.06
RES@DGTPGGLASLENER	*Sorbs1_S432(0:3)*	**1.96**	1.19
LANISVPASES@PR	*Tnks1bp1_S300*	**3.19**	**5.08**
SRNS@PLLDR	*Mark2_S483*	**−1.79**	−1.33
IYHLPDAES@DEDEDFKEQTR	*Sept2_S218*	**1.41**	1.22
KLVIIES@DLERAEER	*Tpm1_S174*	**−9.99**	–
SSHCDS@PPRSQTPQDTNR	*Bnip3_S60*	**−2.33**	−1.34
APS@WIDTGLSEMR	*Cryab_S59*	**3.45**	1.64
AIVSPFHS@PPSTPSSPGIR	*Rcsd1_S120*	**1.77**	1.07
VAKPKS@PEPEATLTFPFLDK	*Limch1_S719*	**−1.37**	1.11
AAVGVTGNDITTPPNKEPPPS@PEKK	*Map4_S667*	**−1.50**	1.01
NKPRPPSLSLLGGHLPSTLSDGPSS@PR	*Trip10_S351*	**−1.89**	1.18
APHSPESPGHSDNPQSSPDSLEAS@PRNPGR	*Perm1_S176*	**−3.26**	1.03
VVANS@PANADYQER	*Ldb3_S112 (isoform 6)*	**−1.60**	−1.05
HQCTSGPIVTLQGNDKSTS@PDPDWSSQLER	*Synpo2_S220*	**−1.72**	−1.08
GCVAS@PVEGGR	*Synpo2_S300*	**−1.45**	−1.07
ILGSAS@PEEEQEKPILDRPTR	*Szrd1_S107*	**1.72**	1.11
AS@GVTVNDEVIK	*Cfl2_S3*	**−1.51**	1.05
RGS@LELGNPSAAHLGDELKEVSTAK	*Svil_S960*	**1.36**	1.39
GLGCSDWKPEAGLS@PPR	*Tcea3_S113*	**−1.48**	1.20
SKPAAADS@EGEEEEEDTAKEKEPPQQGK	*Abcf1_S194*	**1.99**	−1.14
TTS@FAESCKPVQQPSAFGSMK	*Gsk3b_S9*	**4.32**	1.04
MGQAGS@TISNSHAQPFDFPDDSQNAKK	*Gja1_S325*	**−3.24**	−2.23
VKS@PETVKS@PK	*Ttn_S34464,S34470*	**−1.55**	−1.01
VQLLHSQNTS@LINQKK	*Myh6_S1724*	**1.27**	1.21
KVS@KQEEASGGPLAPK	*Vasp_S235*	**1.92**	1.66
GPVS@PPAR	*Naca_S257*	**−1.37**	1.14
KRHS@GDFGADAQGAMSK	*Mb_S121*	**1.57**	1.38
SSS@PVTELTAR	*Srrm2_S1068*	**1.36**	1.07

Table 2 (Continued)

Peptide (@ indicates site of phosphorylation)	Maps to protein phosphorylation site(s)	Fold change relative to old control	
		Young	**Old ELAM**
RS@SDPALTGLSTSVSDNNFSSEEPSR	*Pard3_S143*	**1.29**	1.11
VQLLHS@QNTSLINQK	*Myh6_S1720*	**1.28**	1.51
ATEEPS@GTGS@DELIKSDQVNGV-LVLSLLDK	*Ptrf_S38,S42*	**− 3.39**	− 3.53
EQTAS@APATPLVSK	*Cobll1_S300*	**− 1.47**	1.17
LLQGLLGS@DDEEQEDPKDYCK	*Srpk3_S49*	**− 1.54**	− 1.12
SPS@TIDVVR	*Xirp1_S533*	**3.82**	**1.34**

of the oxidation state of the proteome. This indicates a potential point of convergence in elamipretide's effect on both types of PTMs studied, with thiol redox proteome changes playing a role in regulating the phosphoproteome changes. Confirming which kinases and phosphatases play a role in aging and elamipretide's effects, and whether they are sensitive to oxidative modifications, could be beneficial to further understand cardiac aging and the mechanisms of elamipretide and should be a focus of future research.

Conclusions

These results expand our understanding of how aging impacts the post-translational modification states of cardiac proteins and indicate that elamipretide has a potent effect on the thiol redox status of essential mitochondrial and muscle proteins while also influencing the phosphorylation of various proteins in cardiomyocytes. With these data, we postulate phosphatases could be a potentially critical mediator of elamipretide's effects, a possibility that needs further investigation. In total, the data we have presented here includes many new targets for study in the restoration of cardiac function in old age and has contributed to defining how elamipretide confers its benefits to cardiac healthspan.

Experimental procedures

Animal use and care

All mice used in this study were males of the C57BL/6 strain. Young and Old mice were obtained from the National Institute on Aging Charles River colony and further aged to 5–6 and 24 months, respectively, before starting the study. Mice were housed at 20 °C under diurnal conditions in an AAALAC accredited facility under Institutional Animal Care and Use Committee supervision with ad-libitum access to food and water. Old mice were randomly assigned to Control and elamipretide (Old+ELAM) groups.

Drug administration and treatment groups

Elamipretide was provided by Stealth BioTherapeutics (Needham, MA) and administered at a 3 mg/kg body weight/day dosage through osmotic minipumps (ALZET, Cupertino, CA) implanted surgically under the skin on the left dorsal side of the mice. Old Control mice were implanted with saline-containing pumps. After 4 weeks, the original minipump was surgically removed and a new minipump was implanted to continue the treatment for another 4 weeks.

Euthanasia and tissue handling

Mice were euthanized by live cervical dislocation. Hearts were immediately removed, rinsed with PBS, and weighed. Tissue was cut into ~ 2 mm^3 chunks and snap frozen in liquid N_2 to store for further processing. Frozen tissue was mechanically lysed into a fine powder using a Tissuelyser II (QIAgen, Hilden, Germany) prior to mass spectroscopy-based procedures, with the exception of protein S-glutathionylation.

Large-scale proteome and phoproteome analysis

Sample preparation for proteomic analysis

About 50 mg of ground tissue was resuspended in 1600 µL of lysis buffer composed of 8 M urea,
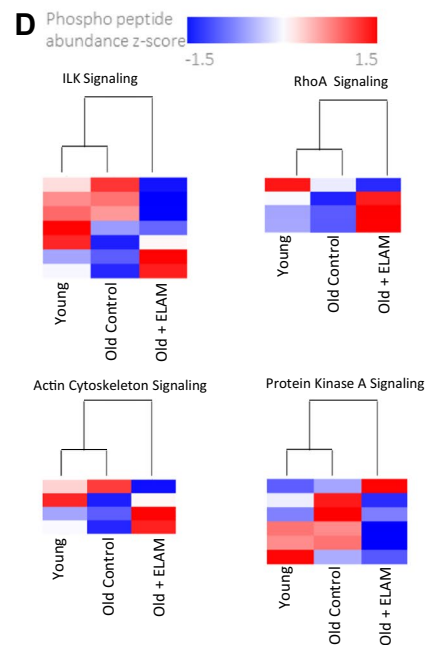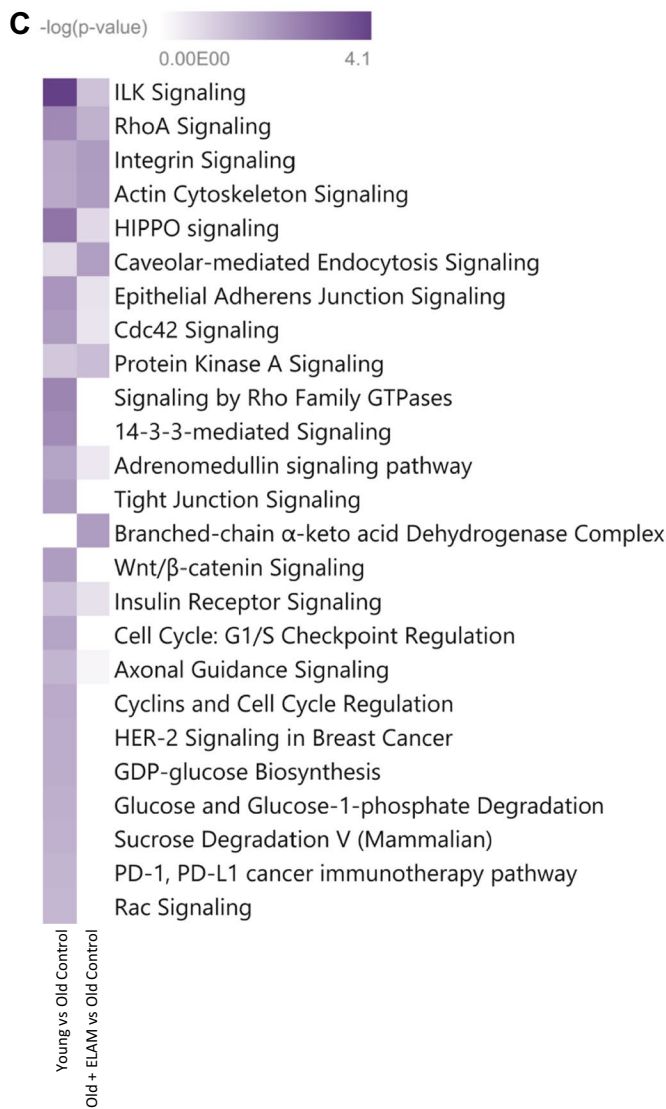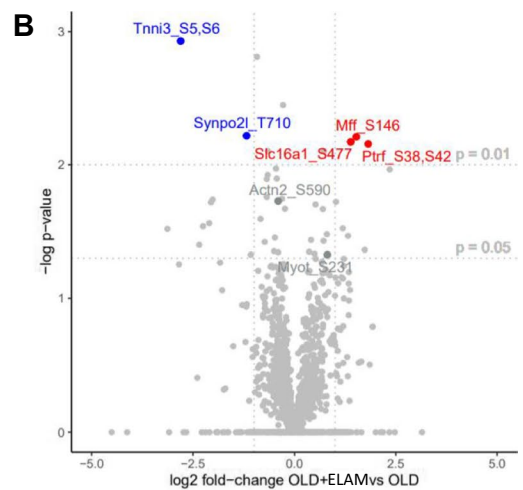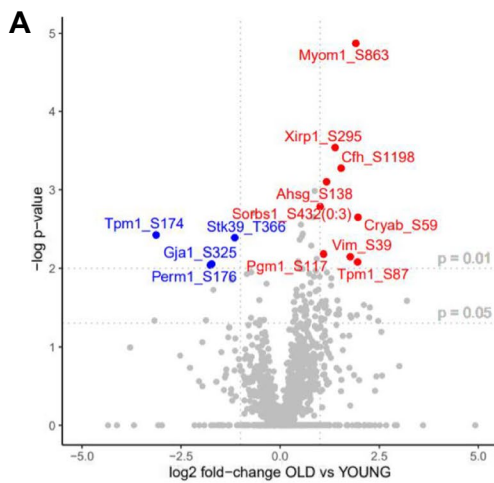
◄**Fig. 2** Analysis of phosphorylation changes in mouse hearts. (**A**, **B**) Volcano plots of protein global phosphorylation analysis. Each dot represents one detected peptide. The horizontal dotted lines indicate unadjusted $P < 0.01$ and $P < 0.05$ as noted on the chart. The vertical dotted lines represent log2 ratios > 1 and < -1. (**C**) P-value heatmap of protein phosphorylation changes in canonical pathways based on all changes with an unadjusted $P < 0.05$. Top 25 pathways, ranked by P-value, are shown. (**D**) Row-normalized z-score heatmaps of significant ($P < 0.05$) S-phosphorylation differences in selected pathways

75 mM NaCl, 50 mM Tris pH 8.2, and a mix of protease inhibitors (Roche Complete EDTA-free) and phosphatase inhibitors (50 mM beta-glycerophosphate, 10 mM sodium pyrophosphate, 1 mM sodium orthovanadate, and 50 mM sodium fluoride). Samples were then subjected to 2 cycles of bead beating (1 min beating, 1.5 min rest) with 0.5-mm diameter zirconia beads and sonicated for 5 min in ice. Samples were centrifuged at 4 °C to remove debris and lysate protein concentration was measured by BCA assay (Thermo Fisher Scientific, Waltham, MA). Protein was reduced with 5 mM dithiothreitol (DTT) for 30 min at 55 °C and alkylated with 15 mM iodoacetamide in the dark for 30 min at room temperature. The alkylation reaction was quenched by incubating with additional 5 mM DTT for 15 min at room temperature. Samples were diluted five-fold with 50 mM Tris pH 8.2. Proteolytic digestion was performed by adding trypsin at 1:200 enzyme to protein ratio and incubating at 37 °C overnight. The digestion was quenched by addition of trifluoroacetic acid to pH 2. Samples were centrifuged to remove insoluble material and peptides were desalted over a 50-mg tC18 SepPak cartridge (Waters Corp, Milford, MA). Briefly, cartridges were conditioned with 1 mL of methanol, 3 mL of 100% acetonitrile, 1 mL of 70% acetonitrile, 0.25% acetic acid and 1 mL of 40% acetonitrile, 0.5% acetic acid; and equilibrated with 3 mL of 0.1% trifluoroacetic acid. Then peptide samples were loaded into the cartridges, washed with 3 mL of 0.1% trifluoroacetic acid and 1 mL of 0.5% acetic acid, and then sequentially eluted first with 0.5 mL of 40% acetonitrile, 0.5% acetic acid and then with 0.5 mL of 70% acetonitrile, 0.25% acetic acid. Twenty micrograms and 500 µg aliquots of eluted peptides were dried by vacuum centrifugation and stored at − 80 °C for proteomic and phosphoproteomic analysis, respectively.

Phosphopeptide enrichment

Phosphopeptide enrichment was done by immobilized metal affinity chromatography (IMAC). Five hundred micrograms of peptides was resuspended in 150µl 80% acetonitrile, 0.1% trifluoroacetic acid. To prepare IMAC slurry, Ni–NTA magnetic agarose (Qiagen) was stripped with 40 mM EDTA for 30 min, reloaded with 10 mM $FeCl_3$ for 30 min, washed 3 times and resuspended in 80% acetonitrile, 0.1% trifluoroacetic acid. Phosphopeptide enrichment was performed using a KingFisher Flex robot (Thermo Fisher Scientific) programmed to incubate peptides with 150µl 5% bead slurry for 30 min, wash 3 times with 150µl 80% acetonitrile, 0.1% trifluoroacetic acid, and elute with 60µl 1:1 acetonitrile:1% ammonium hydroxide. The eluates were acidified with 30µl 10% formic acid, 75% acetonitrile, dried by vacuum centrifugation, and stored at − 80°C until mass spectrometry analysis.

LC–MS/MS analysis

Peptide and phosphopeptide samples were dissolved in 4% formic acid, 3% acetonitrile, loaded onto a 100 µm ID × 3 cm precolumn packed with Reprosil C18 3 µm beads (Dr. Maisch GmbH), and separated by reverse phase chromatography on a 100 µm ID × 30 cm analytical column packed with 1.9 µm beads of the same material and housed into a column heater set at 50 °C. As peptides eluted off the column, they were analyzed online by mass spectrometry. Peptides for proteome analysis were eluted into a Q-Exactive (Thermo Fisher Scientific) mass spectrometer by gradient elution delivered by an EasyII nanoLC system (Thermo Fisher Scientific). The gradient was 9–30% acetonitrile in 0.125% formic acid over the course of 90 min. The total duration of the method, including column wash and equilibration, was 120 min. All MS spectra were acquired on the orbitrap mass analyzer and stored in centroid mode. Full MS scans were acquired from 300 to 1500 m/z at 70,000 FWHM resolution with a fill target of 3E6 ions and maximum injection time of 100 ms. The 20 most abundant ions on the full MS scan were selected for fragmentation using 2 m/z precursor isolation window and beam-type collisional-activation dissociation (HCD) with 26% normalized collision energy. MS/MS spectra were collected at 17,500 FWHM resolution with a fill target of 5E4 ions and maximum injection time of 50 ms. Fragmented
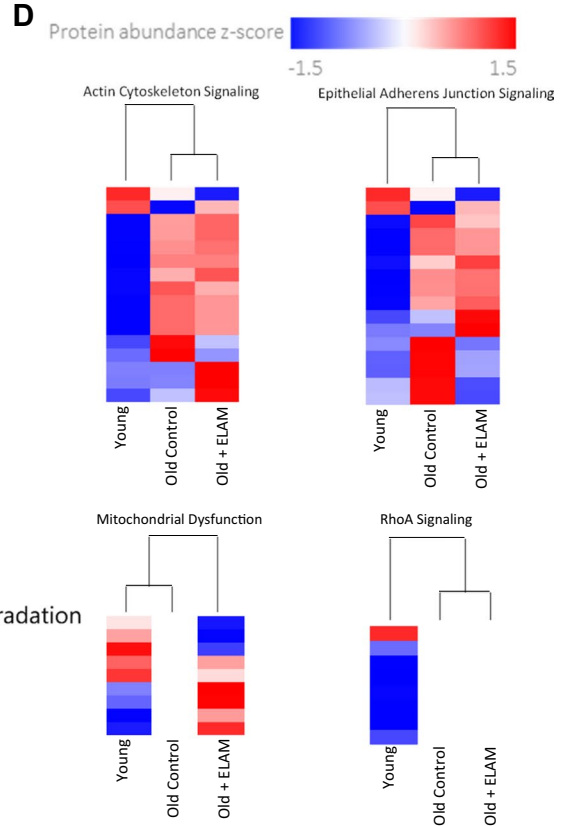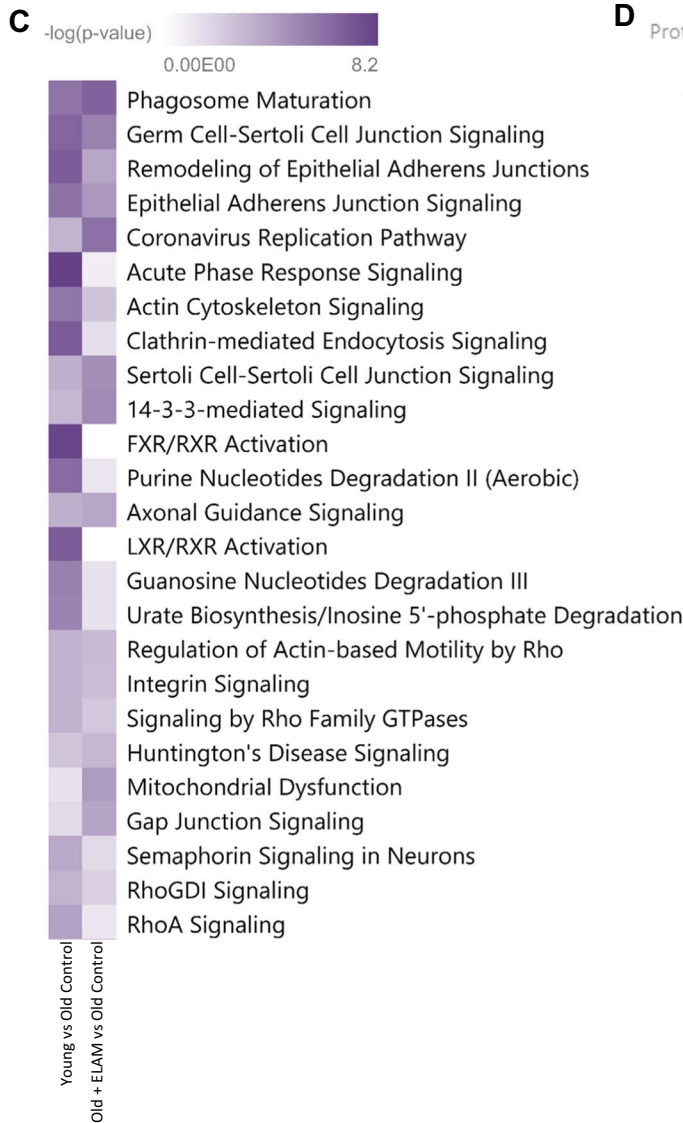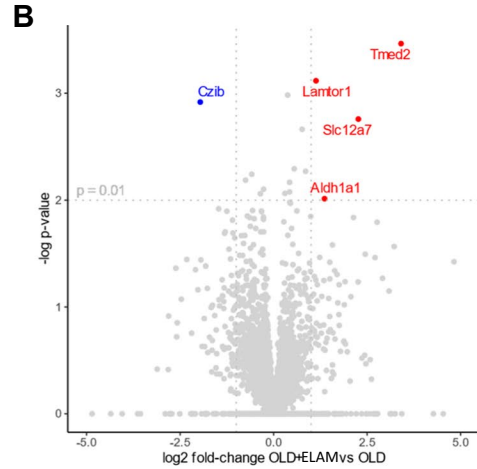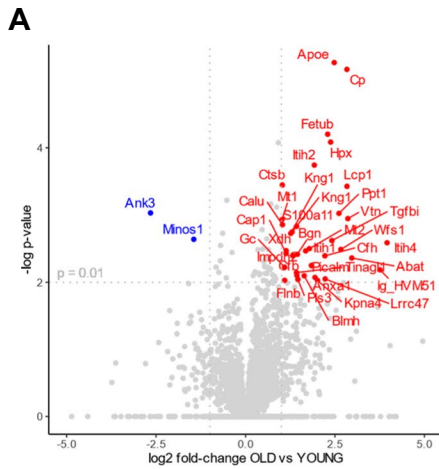
◄**Fig. 3** Analysis of protein abundance changes in mouse hearts. (**A**, **B**) Volcano plots of protein abundance analysis. Each dot represents one protein. The horizontal line indicates FDR < 0.01. (**C**) *P*-value heatmap of protein abundance changes in canonical pathways based on all changes with an unadjusted *P* < 0.05. Top 25 pathways, ranked by *P*-value, are shown. (**D**) Row-normalized z-score heatmaps of significant (*P* < 0.05) protein abundance differences in selected pathways

precursors were dynamically excluded from selection for 30 s. Phosphopeptides for phosphoproteome analysis were eluted into a Velos Orbitrap (Thermo Fisher Scientific) mass spectrometer by gradient elution delivered by an Easy1000 nanoLC system (Thermo Fisher Scientific). The gradient was 9–23% acetonitrile in 0.125% formic acid over the course of 90 min. The total duration of the method, including column wash and equilibration, was 120 min. Full MS scans were acquired in the orbitrap mass analyzer and recorded in centroid mode. Mass range was 300 to 1500, resolution 60,000 FWHM, fill target 3E6 ions, and maximum injection time 100 ms. Each MS scan was followed by up to 20 data-dependent MS/MS scans on the top 20 most intense precursor ions with 2 m/z isolation window, collision-induced dissociation (CID) with 35% normalized collision energy and acquired on the ion trap. Fragmented precursors were dynamically excluded from selection for 30 s.

MS data analysis

Acquired mass spectra raw files were converted to mzXML format and MS/MS spectra were searched against the mouse SwissProt database including isoforms (downloaded May 10, 2015, 24,750 protein sequences) using the Comet search algorithm (version 2015.02 rev.2) [17]. Search parameters included full tryptic enzyme specificity with up to two missed cleavages permitted, mass tolerance of 50 ppm for the precursor and 1 Da for fragments ions, fixed modifications of carbamidomethylation on cysteines, and as variable modifications methionine oxidation and protein N-terminal acetylation. Proteome data is presented based on proteins. Protein Prophet [18] was used for protein inference and the intensities of peptides inferred to the same protein group were summed. A protein group may consist of multiple protein ID's and this information is included in the column named "Indistinguible Proteins" in Appendix 3.

Phosphorylation on serine, threonine, and tyrosine residues was also included as variable modification in phosphoproteome analysis. Peptide matches were filtered to < 1% false-discovery rate, using the target-decoy database strategy and Percolator (version 3.1.2) [19]. Protein inference was carried out using Protein Prophet [18] and protein groups were filtered at ≥ 90% probability score. Peptides were quantified using in-house software by peak-area integration of MS1 spectra, peptide intensities were added for every protein group for protein intensity measurements whereas phosphopeptide intensities were treated individually. Only peptide sequences unique to a protein group were used for quantification. Phosphorylation site localization was performed using an in-house implementation of Ascore [20] and sites with an Ascore > 13 were considered localized, which corresponds to a > 95% probability of correct assignment (*p* < 0.05). If Ascore < 13, the most likely position is indicated including into brackets the range of residues towards the N and C termini of the phosphopeptide where other phospho-acceptor sites reside. Perseus software [21] was used for bioinformatic and statistical analysis using log2 transformed data from total intensity normalized protein intensities and median normalized phosphopeptide intensities from each run.

Targeted PRM phosphoproteomics

Powdered heart tissue was solubilized in 50 mM triethylammonium bicarbonate (TEAB) pH 7.55 buffer with 5% SDS, 2 mM MgCl$_2$, and HALT phosphatase and protease inhibitors (Thermo Fisher Scientific). Eight-hundred nanograms of enolase was added to each 50 μg sample for normalization. Lysates were bound to S-Trap mini columns, washed with TEAB-buffered methanol and a 1:1 mix of chloroform and methanol, digested with trypsin, and eluted following the manufacturer's protocol (Profiti, Farmingdale, NY). Eluents were dried using a CentriVap Concentrator (LABCONCO, Kansas City, MO) and reconstituted in 0.1% formic acid.

One microgram of each sample with 50 femtomole of heavy labeled Peptide Retention Time Calibrant (PRTC) mixture (Thermo Fisher Scientific, cat # 88,321) was loaded onto a 30-cm fused silica picofrit (New Objective, Littleton, MA) 75 μm column and 4 cm 150 μm fused silica Kasil1 (PQ Corporation, Malvern, PA) frit trap loaded with

Table 3 Top 50 age-related protein abundance changes in mouse hearts. Bold indicates unadjusted *P*-value < 0.05. Ordered by lowest *P*-value in Young vs Old Control comparison. Full results can be found in Appendix 3

Protein	Fold change relative to old control	
	Young	Old ELAM
Apoe	**5.57**	− 1.30
Cp	**7.12**	− 1.20
Fetub	**4.91**	− 1.51
Hpx	**5.20**	− 1.25
Tf	**1.89**	1.04
Itih2	**3.79**	− 1.38
Ctsb	**2.04**	− 1.08
Lcp1	**7.13**	− 1.84
Sod2	**− 1.44**	**1.25**
Ahsg	**1.63**	1.13
Cfl1	**1.82**	− 1.23
Ank3	**− 6.30**	1.43
Ppt1	**6.11**	1.25
Vtn	**7.26**	− 1.46
Mt1	**2.02**	− 1.30
Calu	**2.04**	− 1.17
S100a11	**2.69**	**− 1.78**
Hspg2	**1.38**	**− 1.25**
Kng1	**2.46**	− 1.06
Asph	**− 1.56**	1.33
Kng1	**2.40**	− 1.02
Tgm2	**1.51**	− 1.05
Minos1	**− 2.73**	− 1.14
Tgfbi	**5.33**	− 1.21
Itih4	**15.51**	− 1.19
Endog	**− 1.63**	1.06
Mt2	**3.44**	− 1.31
Dusp3	**1.39**	− 1.15
Anxa5	**1.56**	1.05
Wfs1	**6.33**	**− 1.33**
Fabp4	**1.27**	− 1.20
Xdh	**2.20**	− 1.21
Itih1	**3.20**	1.05
Lama2	**− 1.30**	1.04
Cap1	**2.20**	1.10
Bgn	**2.73**	− 1.08
Impdh2	**2.49**	− 1.62
Cfh	**4.65**	1.06
Nt5c3	**1.47**	**− 2.14**
Abat	**7.83**	− 1.30
Cltc	**1.47**	− 1.13
Art3	**− 1.63**	1.36

Table 3 (continued)

Protein	Fold change relative to old control	
	Young	Old ELAM
Rps2	**1.42**	− 1.09
Picalm	**3.58**	− 1.26
Acot7	**1.44**	− 1.62
Gc	**2.13**	1.08
Tppp	**− 1.78**	**1.76**
Ctsd	**1.54**	1.17
Pex3	**1.50**	1.00
Bdh1	**1.63**	**− 1.22**

3 µm Reprosil-Pur C18 (Dr. Maisch) reverse-phase resin analyzed with a Thermo Easy-nLC 1200. The PRTC mixture is used to assess system suitability (QC) before and during analysis. Buffer A was 0.1% formic acid in water and buffer B was 0.1% formic acid in 80% acetonitrile. The 40-min system suitability gradient consisted of a 0 to 16% B in 5 min, 16 to 35% B in 20 min, 35 to 75% B in 1 min, 75 to 100% B in 5 min, followed by a wash of 9 min, and a 30-min column equilibration. The 110-min sample LC gradient consists of a 2 to 7% for 1 min, 7 to 14% B in 35 min, 14 to 40% B in 55 min, 40 to 60% B in 5 min, 60 to 98% B in 5 min, followed by a 9-min wash, and a 30-min column equilibration. Peptides were eluted from the column with a 50 °C heated source (CorSolutions, Ithica, NY) and electrosprayed into a Thermo Orbitrap Fusion Lumos Mass Spectrometer with the application of a distal 3 kV spray voltage. For the sample digest, a full-scan mass spectrum at 60,000 resolution with a mass range of 400 to 2000 m/z, AGC target of 4e5, 50 ms maximum injection time was followed by 81 unscheduled PRM scans at 15,000 resolution with a mass range of 150 to 2000 m/z, AGC target of 5e5, 22 ms maximum injection time, and 27% NCE. Application of the mass spectrometer and LC solvent gradients are controlled by the ThermoFisher XCalibur (version 3.3.2782.34) data system.

Thermo RAW files were converted to mzML format using Proteowizard (version 3.0.19113) and imported into a Skyline document (daily version 20.1.9.234) configured with inclusion peptides (Appendix 3). A DDA with MS1 filtering search was performed using MSAmanda (with built-in Percolator) in Skyline filtering for PRM peptides with a default cut-off of 0.95.
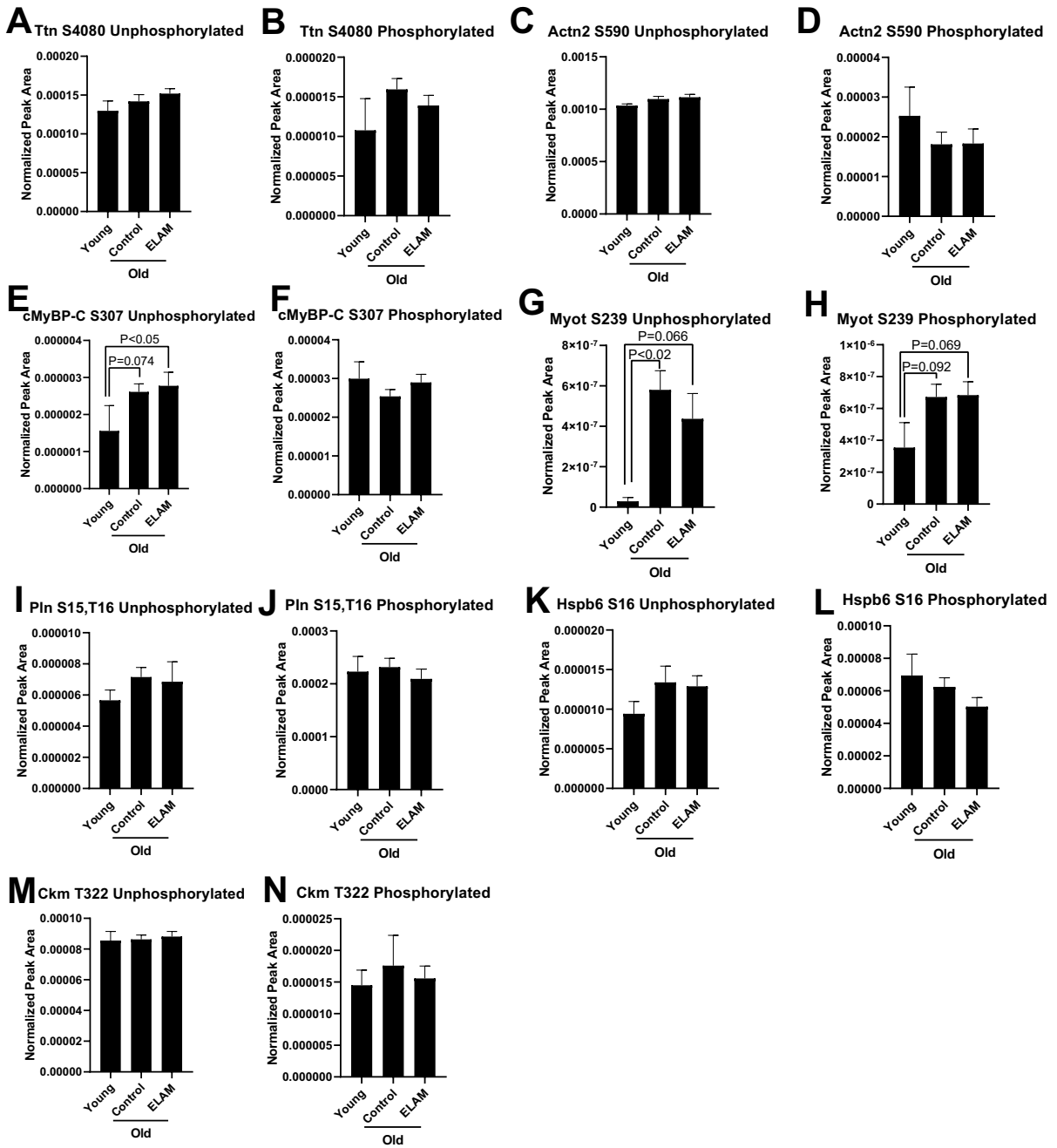
Fig. 4 Parallel reaction monitoring mass spectroscopy of targeted phosphorylation sites in mouse hearts. Sites targeted for analysis were (**A**, **B**) Ttn_S4080, (**C**, **D**) Actn2_S590, (**E**, **F**) cMyBP-C_S307, (**G**, **H**) Myot_S231, (**I**, **J**) Pln_S15,T16, (**K**, **L**) Hspb6_S16, (**M**, **N**) Ckm_T322. Both the phosphorylated and unphosphorylated form of the associated peptide were analyzed for each. Peptide sequences are provided in Table 3. Young $N = 5$, Old Control $N = 21$, Old + ELAM $N = 14$

Parameters used included a fixed carbamidomethyl modification of 57 Da on Cysteine, up to 3 variable phosphorylation modifications of 80 Da on Serine and Threonine, MS1 settings of precursor charge state of 2, and a mass accuracy of 10 ppm with centroided peaks. MS2 settings were fully tryptic allowing for 2 missed

Table 4 Parallel reaction monitoring mass spectroscopy peptide results

Peptide (@ indicates site of phosphorylation)	Maps to protein (site indicated when phosphorylated)	Peptide abundance		
		Young	Old control	Old ELAM
EQANLFSEWLR	Ttn	1.30E-04	1.52E-04	1.42E-04
EQANLFS@EWLR	Ttn_S4080	1.08E-05	1.45E-05	1.59E-05
VIQSYSIR	Actn2	1.03E-03	1.12E-03	1.10E-03
VIQSYS@IR	Actn2_S590	2.53E-05	1.83E-05	1.81E-05
RGTGGVDTAAVGAVFDISNADR	Ckm	8.55E-05	8.81E-05	8.63E-05
RGT@GGVDTAAVGAVFDISNADR	Ckm_T322	1.45E-05	1.56E-05	1.76E-05
RASAPLPGFSAPGR	Hspb6	9.43E-06	1.29E-05	1.34E-05
RAS@APLPGFSAPGR	Hspb6_S16	6.95E-05	5.03E-05	6.25E-05
RDSKLEAPAEEDVWEILR	cMyBP-C	1.56E-06	2.77E-06	2.61E-06
RDS@KLEAPAEEDVWEILR	cMyBP-C_S307	2.99E-05	2.90E-05	2.54E-05
SSSRAEANDQDAIQEK	Myot	2.87E-08	4.37E-07	5.80E-07
SSS@RAEANDQDAIQEK	Myot_S231	3.54E-07	6.84E-07	6.72E-07
RASTIEMPQQAR	Pln	5.66E-06	6.85E-06	7.16E-06
RAS@T@IEMPQQAR	Pln_S15,T16	2.23E-04	2.09E-04	2.32E-04

cleavages, fragment b- and y-ions, retention time filtering of scans within 5 min of MS2 IDs at a tolerance of 10 ppm using the Uniprot mouse canonical FASTA. MSAmanda mzid output files were imported with default cut-off of 0.95 to build a PRM spectral library. Data was then normalized to TIC and mean normalized areas of peptides were exported from Skyline. Due to differences in detection of peptides, only the first batch of samples was able to be quantified for the desired set of peptides. Only peptides that were detected in both the phosphorylated and unphosphorylated state are presented in this paper.

Thiol redox proteomics

A tandem mass tag (TMT)-based quantitative redox proteomics approach was used to measure the relative protein-SSG modification levels in Young, Old Control, and Old + elamipretide heart tissue exactly as described previously for skeletal muscle tissue [22]. This data is reported at the unique cysteine-containing peptide level and the Cys positions for each peptide within the given protein are listed in Appendix 1. In cases where multiple unique peptides correspond to the same Cys positions, we have not summed the multiple peptides to Cys position levels. The availability of multiple peptides for the same Cys positions provided additional information about the rigor of the observed redox changes at these Cys positions for the

given proteins. For peptides that map to multiple proteins in the database, only one protein (first hit) was selected for the output in order to address redundancy.

Protein S-glutathionylation HPLC analysis

Previously snap-frozen heart tissue was homogenized in 1 ml pH 8 HEPES buffer containing 75 mM monobromobimane (MBB). The sample was incubated for 30 min at room temperature to label free thiols with MBB, and then acidified with 10% sulfosalicylic acid (SSA) to precipitate proteins and stabilize GSH-bimane free conjugate. The free thiol supernatant was then removed and the protein pellet was washed 2X with an aliquot of 10% SSA followed by re-solubilization of the protein for 30 min at 60 °C in 0.5 N NaOH. After re-solubilization of the protein pellet the sample was brought to pH 7 with 0.1 N HCL, and the protein-bound glutathione was released by a 30-min incubation in 10 mM tris(2-carboxyethyl)phosphine (TCEP). The solution was then incubated with 1 mM MBB for 30 min. The GSH-bimane conjugate was stabilized by addition of 10% SSA to pH 2, and the sample was then centrifuged to pellet precipitated proteins. A 50-ul aliquot of the supernatant was then injected into a Shimadzu HPLC for quantitation of the GSH-bimane conjugate as previously reported [23], using total protein levels from split samples as the denominator (Bradford protein assay, Bio-Rad, Hercules, CA).

Statistical analysis

Statistical analyses of large-scale proteomics data are described in the above sections. Canonical pathway analysis was performed using Ingenuity Pathway Analysis (IPA) software (QIAgen). PRM results were analyzed by one-way ANOVA as appropriate using Prism software (GraphPad Software, San Diego, CA). All bar charts are plotted as means $\pm$ SEM.

References

1. Morimoto RI, Cuervo AM. Proteostasis and the aging proteome in health and disease. J Gerontol. 2014;69(Suppl 1):S33-8. https://doi.org/10.1093/gerona/glu049.

2. Santos AL, Lindner AB. Protein posttranslational modifications: roles in aging and age-related disease. Oxid Med Cell Longev. 2017;2017:5716409. https://doi.org/10.1155/2017/5716409.

3. Walther DM, Kasturi P, Zheng M, Pinkert S, Vecchi G, Ciryam P, et al. Widespread Proteome Remodeling and Aggregation in Aging C. elegans. Cell. 2015;161(4):919–32. https://doi.org/10.1016/j.cell.2015.03.032.

4. Chiao YA, Zhang H, Sweetwyne M, Whitson J, Ting YS, Basisty N, et al. Late-life restoration of mitochondrial function reverses cardiac dysfunction in old mice. Elife. 2020;9:e55513. https://doi.org/10.7554/eLife.55513.

5. Dai D-F, Chen T, Johnson SC, Szeto H, Rabinovitch PS. Cardiac aging: from molecular mechanisms to significance in human health and disease. Antioxid Redox Signal. 2012;16(12):1492–526. https://doi.org/10.1089/ars.2011.4179.

6. Heron M, Anderson RN. Changes in the leading cause of death: recent patterns in heart disease and cancer mortality. NCHS Data Brief. 2016;254:1–8.

7. Kuka S, Tatarkova Z, Racay P, Lehotsky J, Dobrota D, Kaplan P. Effect of aging on formation of reactive oxygen species by mitochondria of rat heart. Gen Physiol Biophys. 2014;32(03):415–20. https://doi.org/10.4149/gpb_201304 9.

8. Grek CL, Zhang J, Manevich Y, Townsend DM, Tew KD. Causes and consequences of cysteine s-glutathionylation. J

Biol Chem. 2013;288(37):26497–504. https://doi.org/10.1074/jbc.R113.461368 (American Society for Biochemistry and Molecular Biology).

9. Whitson JA, Bitto A, Zhang H, Sweetwyne MT, Coig R, Bhayana S, Shankland EG, Wang L, Bammler TK, Mills KF, Imai S, Conley KE, Marcinek DJ, Rabinovitch PS. SS-31 and NMN: two paths to improve metabolism and function in aged hearts. Aging Cell. 2020;19:e13213. https://doi.org/10.1111/acel.13213.

10. Campbell MD, Duan J, Samuelson AT, Gaffrey MJ, Merrihew GE, Egertson JD, Wang L, Bammler TK, Moore RJ, White CC, Kavanagh TJ, Voss JG, Szeto HH, Rabinovitch PS, MacCoss MJ, Qian WJ, Marcinek DJ. Improving mitochondrial function with SS-31 reverses age-related redox stress and improves exercise tolerance in aged mice. Free Radical Biol Med. 2019;134:268–81. https://doi.org/10.1016/j.freeradbiomed.2018.12.031.

11. Chavez JD, Tang X, Campbell MD, Reyes G, Kramer PA, Stuppard R, Keller A, Marcinek DJ, Bruce JE. Mitochondrial protein interaction landscape of SS-31. BioRxiv. 2019;31: 739128. https://doi.org/10.1101/739128.

12. Mitchell W, Ng EA, Tamucci JD, Boyd KJ, Sathappa M, Coscia A, Pan M, Han X, Eddy NA, May ER, Szeto HH, Alder NN. The mitochondria-targeted peptide SS-31 binds lipid bilayers and modulates surface electrostatics as a key component of its mechanism of action. J Biol Chem. 2020;295(21):7452–69. https://doi.org/10.1074/jbc.RA119.012094.

13. Zhang H, Alder NN, Wang W, Szeto H, Marcinek DJ, Rabinovitch PS. Reduction of elevated proton leak rejuvenates mitochondria in the aged cardiomyocyte. Elife. 2020;9:1–18. https://doi.org/10.7554/ELIFE.60827.

14. Vizcaíno JA, Csordas A, Del-Toro N, Dianes JA, Griss J, Lavidas I, Mayer G, Perez-Riverol Y, Reisinger F, Ternent T, Xu QW, Wang R, Hermjakob H. 2016 update of the PRIDE database and its related tools. Nucleic Acids Res. 2016;44(D1):D447–56. https://doi.org/10.1093/nar/gkv1145.

15 Sohal RS, Orr WC. The redox stress hypothesis of aging. Free Radical Biology and Medicine. 2012;52(3):539–55. https://doi.org/10.1016/j.freeradbiomed.2011.10.445.

16. Loescher CM, Breitkreuz M, Li Y, Nickel A, Unger A, Dietl A, Schmidt A, Mohamed BA, Kötter S, Schmitt JP, Krüger M, Krüger M, Toischer K, Maack C, Leichert LI, Hamdani N, Linke WA. Regulation of titin-based cardiac stiffness by unfolded domain oxidation (UnDOx). Proc Natl Acad Sci USA. 2020;117(39):24545–56. https://doi.org/10.1073/pnas.2004900117.

17. Eng JK, Jahan TA, Hoopmann MR. Comet: an open-source MS/MS sequence database search tool. Proteomics. 2013;13(1):22–4. https://doi.org/10.1002/pmic.201200439.

18. Nesvizhskii AI, Keller A, Kolker E, Aebersold R. A statistical model for identifying proteins by tandem mass spectrometry. Anal Chem. 2003;75(17):4646–58. https://doi.org/10.1021/ac0341261.

19. Käll L, Canterbury JD, Weston J, Noble WS, MacCoss MJ. Semi-supervised learning for peptide identification from shotgun proteomics datasets. Nat Methods. 2007;4(11):923–5. https://doi.org/10.1038/nmeth1113.

20. Beausoleil SA, Villén J, Gerber SA, Rush J, Gygi SP. A probability-based approach for high-throughput protein phosphorylation analysis and site localization. Nat Biotechnol. 2006;24(10):1285–92. https://doi.org/10.1038/nbt1240.

21 Tyanova S, Temu T, Sinitcyn P, Carlson A, Hein MY, Geiger T, Mann M, Cox J. The Perseus computational platform for comprehensive analysis of (prote)omics data. Nature Methods. 2016;13(9):731–40. https://doi.org/10.1038/nmeth.3901.

22. Kramer PA, Duan J, Gaffrey MJ, Shukla AK, Wang L, Bammler TK, Qian WJ, Marcinek DJ. Fatiguing contractions increase protein S-glutathionylation occupancy in mouse skeletal muscle. Redox Biol. 2018;17:367–76. https://doi.org/10.1016/j.redox.2018.05.011.

23 White CC, Krejsa CJ, Eaton DL, Kavanagh TJ. HPLC-based assays for enzymes of glutathione biosynthesis. Curr Prot Toxicol. 1999;1(1):6.5.1-6.5.14. https://doi.org/10.1002/0471140856.tx0605s00.

Publisher's note Springer Nature remains neutral with regard to jurisdictional claims in published maps and institutional affiliations.